

RESEARCH ARTICLE | MAY 20 2025

On the dynamics of equatorial excited dipolar systems

Yangyang Cao ; Alexander Kurganov ; Yongle Liu ; Masoud Rostami ; Vladimir Zeitlin



Physics of Fluids 37, 056618 (2025)

<https://doi.org/10.1063/5.0270628>



Physics of Fluids

Special Topics Open
for Submissions

[Learn More](#)

On the dynamics of equatorial excited dipolar systems

Cite as: Phys. Fluids **37**, 056618 (2025); doi: [10.1063/5.0270628](https://doi.org/10.1063/5.0270628)

Submitted: 12 March 2025 · Accepted: 17 April 2025 ·

Published Online: 20 May 2025



View Online



Export Citation



CrossMark

Yangyang Cao,^{1,a)} Alexander Kurganov,^{2,3,b)} Yongle Liu,^{4,c)} Masoud Rostami,^{3,5,6,d)} and Vladimir Zeitlin⁶

AFFILIATIONS

¹MSU-BIT-SMBU Joint Research Center of Applied Mathematics, Shenzhen MSU-BIT University, Shenzhen 518172, China

²Department of Mathematics, Southern University of Science and Technology (SUSTech), Shenzhen 518055, China

³Shenzhen International Center for Mathematics, Southern University of Science and Technology (SUSTech), Shenzhen 518055, China

⁴Institute of Mathematics, University of Zürich, Winterthurerstrasse 190, 8057, Zürich, Switzerland

⁵Potsdam Institute for Climate Impact Research (PIK), Member of the Leibniz Association, Potsdam, Germany

⁶Laboratoire de Météorologie Dynamique (LMD) / IPSL, ENS-PSL Université, Ecole Polytechnique-Institut Polytechnique de Paris, Sorbonne Université, CNRS, Paris, France

^{a)}Electronic mail: caoyangyang@smbu.edu.cn

^{b)}Electronic mail: alexander@sustech.edu.cn

^{c)}Electronic mail: liuy12017@mail.sustech.edu.cn

^{d)}Author to whom correspondence should be addressed: rostami@pik-potsdam.de and rostami@lmd.ipsl.fr

ABSTRACT

We consider the two-layer moist-convective thermal rotating shallow water equations and design a flux globalization-based, well-balanced, path-conservative central-upwind numerical scheme for the studied model. We use the developed scheme to conduct a series of numerical simulations and report the observation of eastward-propagating *excited dipolar systems*. These systems are characterized by one or more convectively coupled, poorly isolated dipolar fronts, primarily driven by the equatorial adjustment of large-scale localized positive buoyancy or potential temperature anomalies on the equatorial beta plane. A formation of these dynamic structures is triggered when disturbances exceed a critical threshold in a moist-convective environment. Notably, during the evolution of cyclones, secondary counter-rotating anticyclones develop in the lower layer, while oppositely signed structures emerge in the upper layer, highlighting the system's vertical coupling. A significant finding of our experiments is the identification of a *time lag mechanism*, observable even under weaker moist-convective conditions, between the initial state and the system reaching the excited threshold required for eastward propagation. This time lag underscores a critical *build-up phase*, during which the system accumulates the necessary energy and momentum to transition into a dynamically active state.

Published under an exclusive license by AIP Publishing. <https://doi.org/10.1063/5.0270628>

I. INTRODUCTION

Geostrophic adjustment, a fundamental process in atmospheric and oceanic dynamics, describes the evolution of an initially unbalanced flow toward geostrophic equilibrium, where the Coriolis force balances the horizontal pressure gradient force.^{1,2} At the Equator, where the Coriolis parameter is zero and increases linearly with latitude, the adjustment process differs significantly from that in mid-latitude regions. In equatorial dynamics, the vanishing Coriolis force and its sign reversal across the Equator lead to a distinct geostrophic balance, which results in the formation of equatorial wave types, such as Kelvin and Rossby waves. In this study, we employ a two-layer

moist-convective thermal rotating shallow water (mcTRSW) model to investigate the equatorial adjustment of a localized positive temperature anomaly on the equatorial beta-plane, extending the classical framework proposed by Gill.³ A key difference between the rotating shallow water (RSW) and thermal rotating shallow water (TRSW) models is that the latter incorporates horizontal variations in density and/or temperature. Gill's seminal theory, describing the tropical atmosphere's response to localized large-scale heating, predicts the generation of Rossby wave-like propagation to the west and Kelvin wave-like propagation to the east of the heating source. While this framework has profoundly advanced the understanding of tropical

atmospheric dynamics, it does not account for moist convection, which is critical to many equatorial phenomena.

Although the *dry* RSW model has long been used to study equatorial dynamics, its moist-convective counterpart (mcRSW) has only recently been introduced and developed in the literature; see, e.g., Refs. 4–9. One key study using a one-layer mcRSW model revealed notable deviations from Gill's classical mechanism.¹⁰ Specifically, it was shown for the first time that when a large-scale localized negative pressure anomaly exceeds a critical threshold, the adjustment process leads to the formation of an *equatorial modon*—a coherent, horizontally localized dipolar structure propagating slowly eastward while maintaining its shape.¹⁰ This finding provided new insights into the dynamics of equatorial wave systems and the role of threshold-driven adjustments in shaping localized structures. Indeed, it highlights the impact of diabatic processes, such as moist convection, on equatorial dynamics and underscores the limitations of traditional adiabatic interactions are significant. Revisiting classical theories and extending them to include moist-convective effects are essential for advancing the understanding of equatorial phenomena, such as tropical cyclogenesis, the Madden-Julian Oscillation (MJO), and other large-scale convective processes.²

The existence of eastward-moving *equatorial modons*, as a type of *excited dipolar system* with a single front in the RSW beta-plane framework, has been recently reported in Rostami and Zeitlin.^{11,12} This structure has also been investigated on a rotating sphere, further confirming its robustness across different geometries.¹³ Notably, *equatorial modons* can emerge in the TRSW model under asymptotic limits of low divergence and small temperature variations on the equatorial beta-plane.¹⁴ Unlike westward-propagating equatorial solitary waves—also termed modons¹⁵—RSW beta-plane *equatorial modons* propagate eastward, aligning at leading order with the theoretical framework of barotropic quasi-geostrophic (QG) equations on the mid-latitude beta-plane.¹⁶ Indeed, *equatorial modons* also exist in the dry shallow-water model in spherical geometry, where they have been proposed as a key feature of the MJO.¹⁷

Dispersion relations for the barotropic RSW model on a beta-plane highlight the presence of inertio-gravity waves, Kelvin waves, and Rossby waves.¹⁸ However, they fail to explain the slowly eastward-propagating disturbances observed in equatorial circulations, such as the MJO.¹⁹ The MJO, characterized by large-scale convective activity, heavy precipitation, and deep moist convection, is a dominant mode of intraseasonal variability. Originating over the Indian Ocean, it propagates eastward and dissipates over the Pacific Ocean.^{20–22}

The emergence of a dipolar structure in a diabatic, moist-convective environment was first demonstrated in Rostami and Zeitlin²³ by employing the one-layer mcRSW model. Subsequent simulations using a two-layer mcRSW model²³ revealed the generation of slowly eastward-propagating quadrupolar structures driven by disturbances in the lower layer, resembling the structure of the MJO. Building on these foundational findings, a theoretical framework using the mcTRSW model was developed in Rostami *et al.*²⁴ to elucidate the dynamics and genesis of MJO-like structures. This theory shows that eastward-propagating MJO-like structures arise self-sufficiently due to the nonlinear relaxation (adjustment) of large-scale buoyancy anomalies in the presence of moist convection. These episodes exhibit a transient hybrid structure that combines an *equatorial modon* with amplified vortex pairs and a convectively coupled baroclinic Kelvin wave. This system operates on intraseasonal timescales, with the

baroclinic Kelvin wave potentially triggering subsequent MJO-like episodes after completing a circumnavigation of the Equator. The model effectively captures key features of the MJO, including its quadrupolar structure, convective activity, condensation patterns, vorticity fields, phase speed, and the characteristic inflow patterns in the lower and upper troposphere. Subsequent studies, employing the Lagrangian atmospheric model (LAM)²⁵ and the superparameterized community atmosphere model (SPCAM),²⁶ examined the atmospheric response to transient sea surface warming in the equatorial Indian Ocean.²⁷ These simulations demonstrated that such warming consistently triggered the excitation of MJO events, with robust results observed across various experimental setups.²⁷

This study does not aim to comprehensively review MJO theories, which have been addressed in detailed reviews (e.g., Refs. 28 and 29) but rather focuses on specific adjustment scenarios using an improved moist-convective parameterization in the mcTRSW model (Sec. II). While previous mcRSW/mcTRSW studies of equatorial adjustment^{10,23,24} omitted key moist-convective features like downdrafts and cooling effects, we address two fundamental questions: (1) whether excited dipolar structures can emerge in an improved model that rigorously conserves energy and momentum under diabatic conditions, and (2) how the causal sequence between moisture accumulation and MJO initiation operates mechanistically.

Our work introduces four advances beyond the authors' prior studies: (i) identification of a distinct time-lag mechanism and requisite energy build-up phase preceding dipolar system excitation; (ii) development of a novel flux-globalization-based, well-balanced (WB) path-conservative central-upwind (PCCU) numerical scheme; (iii) discovery of multiple frontogenesis events during excited dipolar system emergence; and (iv) implementation of an enhanced mcTRSW framework that resolves essential synoptic-scale equatorial wave interactions while maintaining diagnostic clarity typically lost in full-physics models. This integrated approach yields new mechanistic insights into MJO genesis through systematic isolation and analysis of key dynamical processes in controlled numerical experiments. Our findings indicate that while the dynamics of eastward-propagating MJO-like structures are robust, they are significantly influenced by moist-convective processes and critical parameters, such as lower-layer thickness. Variations in lower-layer thickness affect both the associated dispersion relations and the structural coherence of the *excited dipolar system*. For instance, specific configurations of the lower layer can give rise to multiple *excited dipolar system* fronts, rather than a single dipolar structure resembling an *equatorial modon*, thereby altering the propagation dynamics.

II. MODEL DESCRIPTION AND NUMERICAL METHOD

The dynamical core of the model employed in this study is the two-layer mcTRSW model, as outlined in Rostami *et al.*³⁰ This model extends earlier frameworks, including the one-layer mcTRSW model³¹ and prior two-layer versions.²⁴ The primary advancements lie in a refined moist-convection parameterization that incorporates key physical processes previously overlooked or only partially represented. This refinement balances upward convective fluxes with corresponding downward fluxes near the moist-convective region, achieving a more realistic representation of mass and energy transport and their feedback on the surrounding environment. An additional improvement is the strict enforcement of conservation principles, ensuring that all convective and thermodynamic processes adhere to mass, momentum,

and energy balance laws, thereby enhancing the model's physical relevance. The model also accounts for thermal heating from latent heat release during phase transitions of water vapor to condensed water and captures thermal cooling effects associated with sea surface evaporation. This dual representation enhances the fidelity of both heating and cooling components of moist convection. The two-layer structure of the mcTRSW model represents baroclinic interactions critical for studying phenomena such as equatorial wave dynamics. The lower layer models the denser, moist lower troposphere, while the upper layer captures the dynamics of the upper troposphere, which is assumed to be *dry*. The governing equations of the two-layer mcTRSW model are

$$(v_1)_t + v_1 \cdot \nabla v_1 + f \hat{z} \wedge v_1 = - \left(b_1 \nabla (h_1 + Z) + b_2 \nabla h_2 + \frac{h_1}{2} \nabla b_1 + h_2 \nabla b_2 \right) + \frac{v_2 - v_1}{h_1 b_1} \gamma (C - D), \quad (1)$$

$$(v_2)_t + v_2 \cdot \nabla v_2 + f \hat{z} \wedge v_2 = - \left(b_2 \nabla h_1 + b_2 \nabla (h_2 + Z) + \frac{h_2}{2} \nabla b_2 \right), \quad (2)$$

$$(h_1)_t + \nabla \cdot (h_1 v_1) = \frac{1}{b_1} \gamma (C - D), \quad (3)$$

$$(h_2)_t + \nabla \cdot (h_2 v_2) = \frac{1}{b_2} \gamma (-C + D), \quad (4)$$

$$(b_1)_t + v_1 \cdot \nabla b_1 = \frac{1}{h_1} (-C + D), \quad (5)$$

$$(b_2)_t + v_2 \cdot \nabla b_2 = \frac{1}{h_2} (C - \mu E), \quad (6)$$

$$Q_t + \nabla \cdot (Q v_2) = -C + E, \quad (7)$$

where x and y are zonal and meridional coordinates, $(x, y) \in \Omega$, t is time, $\nabla := (\partial/\partial x, \partial/\partial y)$, \hat{z} is the unit vector in the vertical direction, $v_i(x, y, t) = (u_i(x, y, t), v_i(x, y, t))^T$ are the horizontal velocities, $u_i(x, y, t)$ and $v_i(x, y, t)$, $i = 1, 2$, are the zonal and meridional velocities of the corresponding layers counted from the top, $h_1(x, y, t)$ and $h_2(x, y, t)$ denote the thicknesses of the upper and lower layers, respectively, $b_1 = g \frac{\theta_1}{\theta_0}$ and $b_2 = g \frac{\theta_2}{\theta_0}$ are the layer-averaged buoyancy variables, where θ_1 and θ_2 are the corresponding potential temperatures at the upper and lower layers, θ_0 is the reference constant potential temperature, g is a constant acceleration due to gravity, Z is the bottom topography, and $f(y) = f_0 + \beta y$ is the Coriolis parameter with f_0 and β being constants (for the equatorial case of this study, $f_0 = 0$). In the moisture Eq. (7), Q is rescaled columnar bulk humidity in the lower layer,³⁰ and $C = \frac{Q - Q_s}{\tau} \mathcal{H}(Q - Q_s)$ and $E = \alpha \frac{|v_2|}{|(v_2)_{\max}|} (Q_s - Q) \mathcal{H}(Q_s - Q)$ represent condensation and sea surface evaporation, where \mathcal{H} is the Heaviside function, α is an adjustment coefficient, $|(v_2)_{\max}| := \max_{x,y} |v_2(x, y, t)|$, and D denotes downward motion, akin to a downdraft in the adiabatic convective process: $D = \frac{1}{\tau} \int \int C \, dx dy$, where κ is a fraction of Ω , in which $0.97Q_s < Q < Q_s$. Notably, a recent advancement for mcTRSW systems is the development of an alternative sea surface evaporation scheme that explicitly incorporates both temperature and lower-layer velocity field dependencies.³² We assume that the water vapor in the lower layer is close to saturation and in the upper layer far from saturation. When the bulk humidity exceeds a saturation threshold, condensation starts, introducing a sink

in Eqs. (4) and (5) and a source in Eqs. (3) and (6). In addition, τ is the condensation parameter, γ is a constant parameter that adjusts the impact of the balance between heating and cooling, and updraft and downdraft processes, $\mu = \frac{\int \int C \, dx dy}{\int \int E \, dx dy}$ is a parameter that provides a balance between E , as a source of moisture in the lower layer, and C . Equations (1)–(7) can be put into the following conservative form:

$$(h_1)_t + (h_1 u_1)_x + (h_1 v_1)_y = \frac{\gamma(C - D)}{b_1}, \quad (8)$$

$$(q_1)_t + \left(h_1 u_1^2 + \frac{1}{2} b_1 h_1^2 \right)_x + (h_1 u_1 v_1)_y = f h_1 v_1 - h_1 (h_2 b_2)_x - h_1 b_1 Z_x + u_2 \frac{\gamma(C - D)}{b_1}, \quad (9)$$

$$(p_1)_t + (h_1 u_1 v_1)_x + \left(h_1 v_1^2 + \frac{1}{2} b_1 h_1^2 \right)_y = -f h_1 u_1 - h_1 (h_2 b_2)_y - h_1 b_1 Z_y + v_2 \frac{\gamma(C - D)}{b_1}, \quad (10)$$

$$(h_1 b_1)_t + (h_1 u_1 b_1)_x + (h_1 v_1 b_1)_y = -\frac{(1 - \gamma)(C - D)}{b_1}, \quad (11)$$

$$(h_2)_t + (h_2 u_2)_x + (h_2 v_2)_y = -\frac{\gamma(C - D)}{b_2}, \quad (12)$$

$$(q_2)_t + \left(h_2 u_2^2 + \frac{1}{2} b_2 h_2^2 \right)_x + (h_2 u_2 v_2)_y = f h_2 v_2 - h_2 b_2 (h_1)_x - h_2 b_2 Z_x - u_2 \frac{\gamma(C - D)}{b_2}, \quad (13)$$

$$(p_2)_t + (h_2 u_2 v_2)_x + \left(h_2 v_2^2 + \frac{1}{2} b_2 h_2^2 \right)_y = -f h_2 u_2 - h_2 b_2 (h_1)_y - h_2 b_2 Z_y - v_2 \frac{\gamma(C - D)}{b_2}, \quad (14)$$

$$(h_2 b_2)_t + (h_2 u_2 b_2)_x + (h_2 v_2 b_2)_y = \frac{(1 - \gamma)(C - D)}{b_2} + D - \mu E, \quad (15)$$

$$Q_t + (Q u_2)_x + (Q v_2)_y = -C + E, \quad (16)$$

where $q_i := h_i u_i$ and $p_i := h_i v_i$ are the x - and y -discharges, respectively, for the i th component of the system ($i = 1, 2$).

The multilayer TRSW model has a robust theoretical foundation that dates back to the 1990s (e.g., Refs. 2 and 33), but its practical applications have emerged only in recent years. This delay stems primarily from the lack of reliable numerical methods capable of addressing the inherent challenges of TRSW systems. One significant issue is the potential loss of hyperbolicity, which can lead to Kelvin–Helmholtz-type instabilities—a genuine physical phenomenon rather than a numerical artifact. Another challenge in development of reliable numerical methods for TRSW systems is a delicate balance between the fluxes and source terms: a good scheme should be well-balanced (WB) in the sense that it should be capable of exactly preserving (some of physically relevant) steady states. Achieving the WB property within a rotating frame further complicates numerical modeling. Additionally, resolving sharp fronts or hydraulic jumps, as required in TRSW or mcTRSW systems, presents substantial challenges. Another

critical difficulty arises from the presence of nonconservative products in the system (8)–(16). These terms are not well-defined in the distributional framework. Instead, weak solutions must be interpreted as Borel measures.^{34,35} To address this issue, nonconservative terms can be effectively handled using a path-conservative approach introduced in Ref. 36 and further developed in Castro *et al.*,³⁷ see also Castro *et al.*,³⁸ and Parés.³⁹ This methodology has enabled significant advancements in the numerical treatment of hyperbolic systems with nonconservative products, making the TRSW model feasible for practical and accurate simulations.

To overcome the aforementioned challenges, we employ a flux globalization based WB path-conservative central-upwind (PCCU) scheme proposed in Cao *et al.*^{40,41} for two-layer TRSW equations. To extend this scheme to the moist-convective case, we write the mcTRSW system (8)–(16) in the following form:

$$\mathbf{U}_t + \mathbf{K}(\mathbf{U})_x + \mathbf{L}(\mathbf{U})_y = \mathbf{M}(\mathbf{U}), \quad (17)$$

$$\mathbf{K}(\mathbf{U}) = \mathbf{F}(\mathbf{U}) - \mathcal{R}(\mathbf{U}),$$

$$\mathcal{R}(\mathbf{U}) = \int_{\hat{x}}^x \mathbf{S}^x(\mathbf{U}(\xi, y, t), \mathbf{U}_{\xi}(\xi, y, t), \mathbf{U}_y(\xi, y, t)) d\xi, \quad (18)$$

$$\mathbf{L}(\mathbf{U}) = \mathbf{G}(\mathbf{U}) - \mathbf{R}(\mathbf{U}),$$

$$\mathbf{R}(\mathbf{U}) = \int_{\hat{y}}^y \mathbf{S}^y(\mathbf{U}(x, \eta, t), \mathbf{U}_x(x, \eta, t), \mathbf{U}_{\eta}(x, \eta, t)) d\eta, \quad (19)$$

where \hat{x} and \hat{y} are arbitrary numbers, $\mathbf{U} = (h_1, q_1, p_1, h_1 b_1, h_2, q_2, p_2, h_2 b_2, Q)^{\top}$, \mathbf{K} and \mathbf{L} are global fluxes with

$$\mathbf{F}(\mathbf{U}) = \left(q_1, \frac{q_1^2}{h_1} + \frac{b_1}{2} h_1^2, \frac{q_1 p_1}{h_1}, q_1 b_1, q_2, \frac{q_2^2}{h_2} + \frac{b_2}{2} h_2^2, \frac{q_2 p_2}{h_2}, q_2 b_2, \frac{Q q_2}{h_2} \right)^{\top}, \quad (20)$$

$$\mathbf{G}(\mathbf{U}) = \left(p_1, \frac{q_1 p_1}{h_1}, \frac{p_1^2}{h_1} + \frac{b_1}{2} h_1^2, p_1 b_1, p_2, \frac{q_2 p_2}{h_2}, \frac{p_2^2}{h_2} + \frac{b_2}{2} h_2^2, p_2 b_2, \frac{Q p_2}{h_2} \right)^{\top}, \quad (21)$$

$$\mathbf{S}^x = (0, f h_1 v_1 - h_1 (h_2 b_2)_x - h_1 b_1 Z_x, 0, 0, 0, f h_2 v_2 - h_2 b_2 (h_1)_x - h_2 b_2 Z_x, 0, 0, 0)^{\top}, \quad (22)$$

$$\mathbf{S}^y = (0, 0, -f h_1 u_1 - h_1 (h_2 b_2)_y - h_1 b_1 Z_y, 0, 0, 0, -f h_2 u_2 - h_2 b_2 (h_1)_y - h_2 b_2 Z_y, 0, 0)^{\top}, \quad (23)$$

and \mathbf{M} represents the source terms, which were not present in the *dry* TRSW equations

$$\mathbf{M}(\mathbf{U}) = \left(\frac{\gamma(C-D)}{b_1}, u_2 \frac{\gamma(C-D)}{b_1}, v_2 \frac{\gamma(C-D)}{b_1}, -\frac{(1-\gamma)(C-D)}{b_1}, \right. \\ \left. u_2 \frac{\gamma(C-D)}{b_2}, -v_2 \frac{\gamma(C-D)}{b_2}, \frac{(1-\gamma)(C-D)}{b_2} + D, \right. \\ \left. -\mu E, -C + E \right)^{\top}.$$

We then introduce a uniform mesh consisting of the finite-volume cells $C_{j,k} := [x_{j-\frac{1}{2}}, x_{j+\frac{1}{2}}] \times [y_{k-\frac{1}{2}}, y_{k+\frac{1}{2}}]$ with $x_{j+\frac{1}{2}} - x_{j-\frac{1}{2}} \equiv \Delta x$ and

$y_{k+\frac{1}{2}} - y_{k-\frac{1}{2}} \equiv \Delta y$ for all j, k . Assume that the computed solution, realized in terms of its cell averages

$$\bar{U}_{j,k}(t) \approx \frac{1}{\Delta x \Delta y} \iint_{C_{j,k}} U(x, y, t) dx dy, \quad (24)$$

are known at a certain time t . We evolve them in time by solving the following system of ODEs

$$\frac{d}{dt} \bar{U}_{j,k} = - \frac{\mathcal{K}_{j+\frac{1}{2},k}(t) - \mathcal{K}_{j-\frac{1}{2},k}(t)}{\Delta x} - \frac{\mathcal{L}_{j,k+\frac{1}{2}}(t) - \mathcal{L}_{j,k-\frac{1}{2}}(t)}{\Delta y} \\ + \mathcal{M}_{j,k}(t), \quad (25)$$

where $\mathcal{K}_{j+\frac{1}{2},k}$ and $\mathcal{L}_{j,k+\frac{1}{2}}$ are the WB PCCU global numerical fluxes given in Cao *et al.*,⁴¹ and

$$\mathcal{M}_{j,k} \approx \frac{1}{\Delta x \Delta y} \iint_{C_{j,k}} \mathbf{M}(\mathbf{U}(x, y, t)) dx dy, \quad (26)$$

which is discretized using a midpoint rule. The ODE system (25) is integrated in time using a semi-implicit strong stability preserving method from Chertock *et al.*⁴² with the semi-implicit treatment applied only to the stiff term on the right-hand side of the moisture Eq. (16), namely, to the term $-\frac{Q-Q_s}{\tau} \mathcal{H}(Q - Q_s)$.

III. RESULTS

This section presents the results of equatorial adjustment to a large-scale buoyancy anomaly in the lower layer, initialized with an alpha-Gaussian shape,⁸ with no initial perturbation in the upper layer. The initial buoyancies for the lower and upper layers are given by

$$b_1(x, y, 0) \equiv 2, \quad b_2(x, y, 0) = 1 + 0.3 \frac{G(r) - G(\infty)}{G(0) - G(\infty)}, \quad r = \sqrt{x^2 + 4y^2}, \quad (27)$$

where $G(r) = \int_{0.5r^3}^5 e^{-t} t^{-1/6} dt$, $G(\infty) \approx -0.40$, and $G(0) \approx 0.72$; see Fig. 1. This anomaly exhibits symmetry with respect to the Equator in both *dry* and moist-convective scenarios. The alpha-Gaussian shape offers a smooth, localized buoyancy anomaly that mimics the spatial extent of tropical convective heating. In addition, specifically chosen b_1 and b_2 serve to represent a strong lower-layer perturbation against a

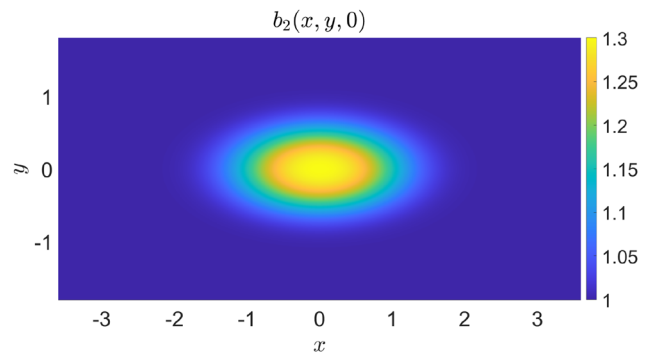


FIG. 1. Initial buoyancy anomaly in the lower layer with an alpha-Gaussian shape, symmetric about the Equator. The upper layer remains unperturbed.

TABLE I. Configuration of the numerical experiments. The last column specifies whether *dry* conditions or moist convection are included. In all cases, the nondimensionalized Coriolis parameter is set as $f = \gamma$. For the experiments involving moist convection, the parameters are $Q_s = 0.6$, $\tau = 0.7$, $\gamma = 0.9$, and $\alpha = 0.3$.

Case	$h_1(x, y, 0)$	$h_2(x, y, 0)$	$q_1(x, y, 0)$	$p_2(x, y, 0)$	$q_2(x, y, 0)$	$p_2(x, y, 0)$	$Q(x, y, 0)$	
1	0.65	0.35	0	0	0	0	$Q_s - 0.01$	Moist
2	0.60	0.40	0	0	0	0	$Q_s - 0.01$	Moist
3	0.65	0.35	0	0	0	0		Dry

relatively quiescent upper layer, thereby isolating the dynamics of interest.

The simulations are performed over the computational domain $[-5.5, 5.5] \times [-10, 10]$, discretized with 400×500 uniform cells. Homogeneous Neumann boundary conditions are applied at $y = \pm 10$ boundaries to allow for the evacuation of short inertia-gravity waves, while periodic boundary conditions are applied in the x -direction to capture the effects of circumnavigating Kelvin waves on the equatorial adjustment of the perturbation.

The length and time scales in this study are nondimensionalized using the equatorial Rossby deformation radius, namely, $(x, y) \sim L_d = \sqrt{\frac{c}{\beta}}$, $t \sim \frac{1}{\beta L_d}$, where $(u, v) \sim c = \sqrt{BH}$, and B is the buoyancy and H are the thickness scales, respectively, and β is the gradient of the Coriolis force in the meridional direction.

Table I defines the three initialization cases examined in this study. Case 1 shares the same initialization as case 3 but occurs in a moist-convective environment. In contrast, case 3 is set in a *dry*, adiabatic environment. This mechanism describes the tropical atmospheric response to localized heating, producing an east-west asymmetry in circulation. East of the heating, fast-propagating Kelvin waves symmetrically move eastward, while westward-propagating Rossby waves dominate on the western side, with slower, geostrophically balanced adjustments. This asymmetry forms the basis for large-scale phenomena such as the Walker circulation and monsoons. As it was demonstrated in Rostami and Zeitlin,¹⁰ in the region west of localized heating, in addition to Rossby waves, circular equatorial anomalies can generate signals corresponding to faster westward-propagating inertia-gravity waves (WIGWs), which are significantly larger than their equatorially elongated counterparts. These WIGWs, characterized by the lowest meridional mode, are distinctly observable in the velocity field and precede the slower-propagating Rossby wave signals. According to non-dissipative asymptotic theory, an arbitrary long-wave equatorial perturbation with a small characteristic Rossby number naturally decomposes into fast and slow components.^{43–45} The fast component, comprising inertia-gravity and Yanai waves, is governed by two critical factors: a Doppler shift induced by interactions with the slow components and a nonlinear frequency shift resulting from the system's inherent nonlinearity.⁴⁴ Similarly, geostrophic adjustment in mid-latitudes also exhibits a dynamical splitting between fast inertia-gravity waves and slow quasi-geostrophic motions; see, e.g., Refs. 46–48.

Figures 2 and 3 illustrate the evolution of the vorticity field across the three cases. Kelvin waves, being inherently non-rotational, generate negligible vorticity fields, as they are primarily driven by gravity and propagate along the Equator without inducing significant rotational motion in the surrounding fluid. In contrast, Rossby waves are strongly associated with vorticity variations due to their dependence on Earth's

rotation and the conservation of potential vorticity under adiabatic conditions.

Cases 1 and 2, occurring in a moist-convective environment, show substantial deviations from the *dry* case 3. At the onset of the adjustment process, an almost isotropic inflow converges toward the center of the buoyancy anomaly. Over time, the beta effect alters the direction of these inflows, leading to the formation of a circular motion. In the presence of moist convection, these symmetric circular motions about the Equator intensify, resulting in the development of eastward-propagating twin cyclones. The formation of an *excited dipolar system*, capable of generating secondary anticyclones and eventually establishing a quadrupole structure in a two-layer baroclinic system—characterized by opposite vorticity signs in the upper layer—requires a moist-convective environment.

As the cyclonic structures evolve, vorticity convergence increases near the central anomaly, particularly in the moist-convective cases. This frontogenesis in the lower layer leads to a significant intensification of cyclonic circulation, which is more pronounced in case 1 due to higher convective energy flux.

In contrast, under *dry* conditions, even in the presence of substantial atmospheric anomalies, the system's dynamics are primarily governed by the classical Gill mechanism. In such cases, no eastward-propagating dipolar structures are observed. Notably, the vorticity signature of the *excited dipolar system* is significantly stronger than that of the Rossby waves. During its genesis, the vorticity in some regions can reach magnitudes approximately an order of magnitude higher than that of the Rossby waves.

While weak-amplitude anomalies in moist-convective environments replicate a Gill-like response, characterized by east-west asymmetry in atmospheric circulation, larger-amplitude anomalies give rise to enhanced *excited dipolar systems* that resemble quasi-equatorial modons. These modons, as described in Rostami and Zeitlin,^{10,11} Zhao *et al.*,¹³ are robust, self-sustained dipolar vortices capable of propagating coherently over substantial distances. This structural transition underscores the nonlinear scaling behavior of the system: as the amplitude increases in a diabatic environment, the system shifts from a linear response (Gill-like) to a nonlinear regime (modon-like), exhibiting distinct dynamical characteristics.

Another notable feature of these results, compared to the findings in Rostami and Zeitlin,¹¹ is the emergence of multiple fronts of twin cyclones. In our simulations, these fronts initially develop when cyclonic anomalies in the lower layer intensify due to enhanced moisture convergence and latent heat release. As these cyclonic components elongate along the zonal direction, they begin to extend eastward under the influence of the ambient flow. Over time, the continuous stretching and differential advection lead to a bifurcation process, or splitting, of these elongated cyclonic structures,⁴⁹ yielding two distinct cyclones with differing dynamical characteristics. The cyclone situated

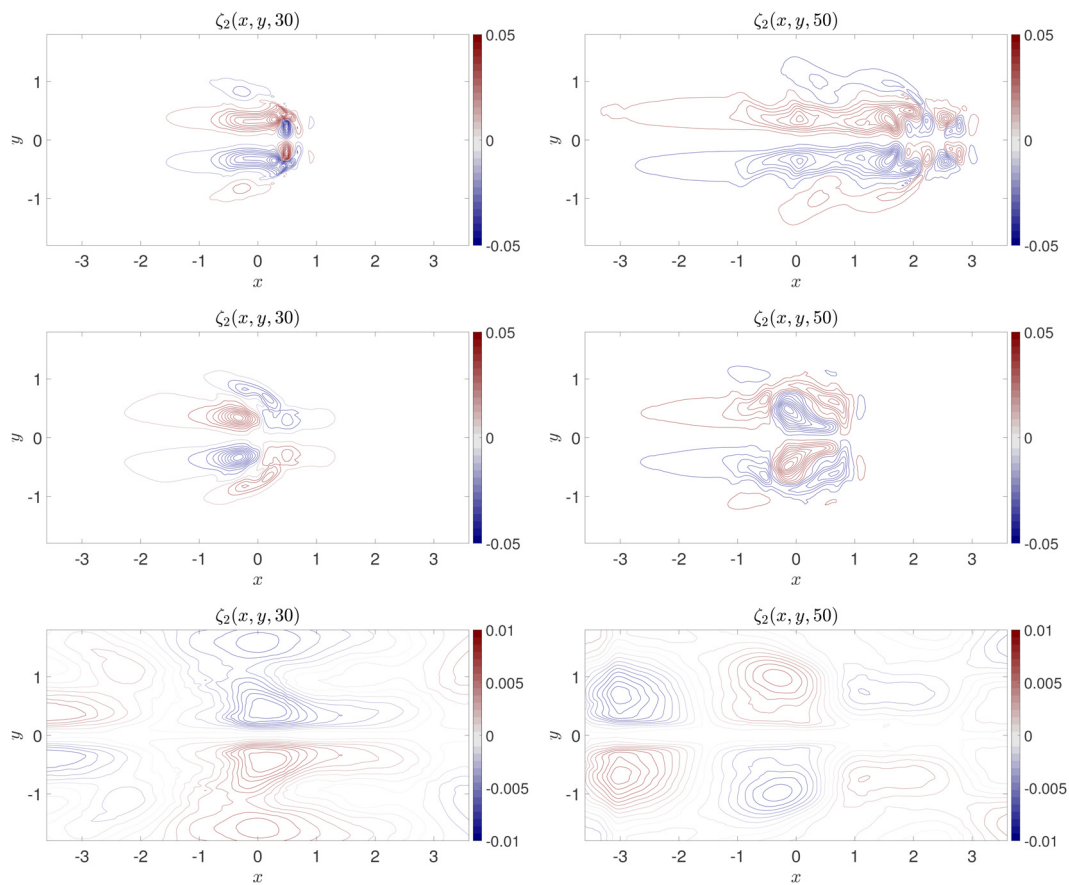


FIG. 2. Evolution of the relative vorticity field $\zeta_2 := (v_2)_x - (u_2)_y$ in the lower layer at $t = 30$ (left column) and $t = 50$ (right column) in cases 1 (upper row), 2 (middle row), and 3 (bottom row). The moist-convective cases exhibit distinct dipolar structures, with case 1 showing enhanced eastward propagation and the formation of twin cyclones. In contrast, the dry case 3 produces weaker, less organized dipolar patterns.

on the western side of the split exhibits a marked decrease in intensity shortly after formation. This weakening phase is associated with reduced convective heating and enhanced entrainment of drier air from the surroundings. Consequently, its dynamical behavior transitions to that dominated by slower-moving, rotational dynamics characteristic of Rossby waves. These waves, with their larger spatial scales and lower propagation speeds, signal a reorganization of energy into more balanced, vorticity-dominated modes. Conversely, the eastern cyclone maintains its coherence and robust structure as it continues to propagate eastward. The sustained convective activity and favorable environmental conditions allow this cyclone to preserve its intensity, even as it intermittently generates secondary small-scale vortices. Such secondary features are indicative of localized shear instabilities and the nonlinear interactions between convective plumes, which help to modulate the overall energy distribution within the system; see Fig. 2, upper row.

The splitting of cyclonic components and the subsequent formation of secondary vortices in our simulations may correspond to the mesoscale and synoptic disturbances often observed within the broader MJO envelope. This behavior suggests that the processes of cyclogenesis and vortex interaction are intricately linked to the

multiscale dynamics that govern tropical variability. Moreover, the distinct propagation characteristics of the twin cyclones align well with observational studies. For instance, Wang *et al.*⁵⁰ identified four archetypal propagation patterns in the MJO, namely: standing, jumping, slow eastward propagation, and fast eastward propagation. Our simulation results corroborate these classifications and further hint at a mechanism, by which the interplay between convective heating, vortex splitting, and baroclinic interactions may lead to the diversity of observed MJO propagation regimes.

We observed that the upper-layer vorticity initially remains weak, but as the dipolar structures form and propagate, the upper layer becomes increasingly influenced by the evolving lower-layer dynamics, especially under moist-convective conditions. This influence is particularly evident in the emergence of secondary vortices within the upper layer as the system evolves; see Fig. 3.

Importantly, when the initial amplitude of the lower-layer thickness increases while maintaining the same aspect ratio and other initial conditions, the adjustment scenario changes significantly; see middle rows in Figs. 2 and 3. Enhanced dipolar structures with reduced thickness and higher vorticities propagate eastward at faster rates, underscoring the sensitivity of adjustment dynamics to the amplitude of the

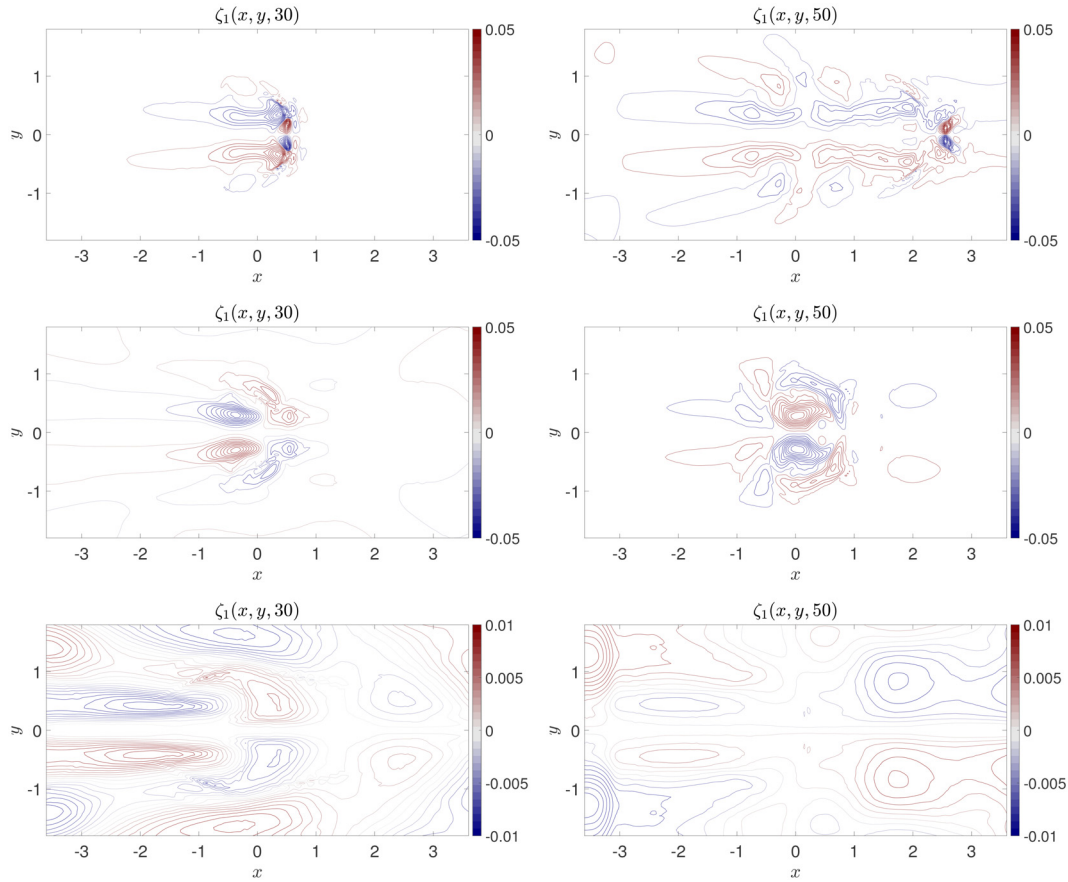


FIG. 3. Same as in Fig. 2, but for the upper layer.

initial condition. For localized initial disturbances on the equatorial beta-plane, the non-dissipative asymptotic theory has inherent limitations due to the breakdown of Kelvin waves.⁴⁴ While these limitations have minimal impact on the westward-moving Rossby wave component, as Kelvin waves propagate in the opposite direction, the eastward-moving component is particularly susceptible to disruption from Kelvin wave overturning. This breakdown complicates the accurate calculation of eastward-propagating results using asymptotic expansions and highlights the enhanced role of nonlinearity, particularly in moist-convective environments. The nonlinear effects significantly influence the splitting and subsequent evolution of eastward-propagating dipolar fronts in the system.

The evolution of the nondimensional absolute vorticity in the mcTRSW model³⁰ is governed by

$$(\partial_t + \mathbf{v}_i \cdot \nabla)(\zeta_i + f) = \mathcal{J}(\tilde{h}_i, b_i) - \frac{1}{b_i}(\zeta_i + f)\alpha_i, \quad (28)$$

where ζ_i is the relative vorticity, $\tilde{h}_1 = Z + \frac{1}{2}h_1$, $\tilde{h}_2 = Z + h_1 + \frac{1}{2}h_2$, and \mathcal{J} represents the Jacobian operator. The term α_i is proportional to $-C + D$. This proportionality introduces the effects of moist convection into the vorticity dynamics. In regions of condensation, $\alpha_i < 0$, this leads to an intensification of cyclonic vorticity. Conversely, in

regions dominated by downward drafts, $\alpha_i > 0$, the moist-convective effects result in a weakening of cyclonic vorticity within the corresponding layer.

Figures 4 and 5 clearly illustrate a notable disparity in the intensification of dipolar cyclones and zonal velocity between the moist-convective cases and the *dry* case, as reflected in the zonally averaged (in x and in time from $t = 30$ to 50) values of these variables. In the lower layer, cyclonic motion dominates, whereas anticyclonic motion is predominant in the upper layer.

A distinct feature of the *excited dipolar systems* in case 1 is the zonally averaged buoyancy potential temperature anomaly distribution (Fig. 4, upper left panel), which reveals a dual-peak structure situated off the Equator, near the regions of extrema relative vorticity in the lower layer. This contrasts with cases 2 and 3, where the maximum buoyancy anomaly is concentrated around the Equator. A local empirical orthogonal function (EOF) analysis over the equatorial region of the Eastern Hemisphere (0° – 180° E) identifies two principal components corresponding to the eastward propagation of a dipolar vortex constrained to the Equator.⁵¹ These findings are consistent with the vorticity evolution observed in the *excited dipolar systems* analyzed in this study. In contrast, in case 2, which represents a semi-excited quadrupole structure, the buoyancy anomaly is more symmetric with

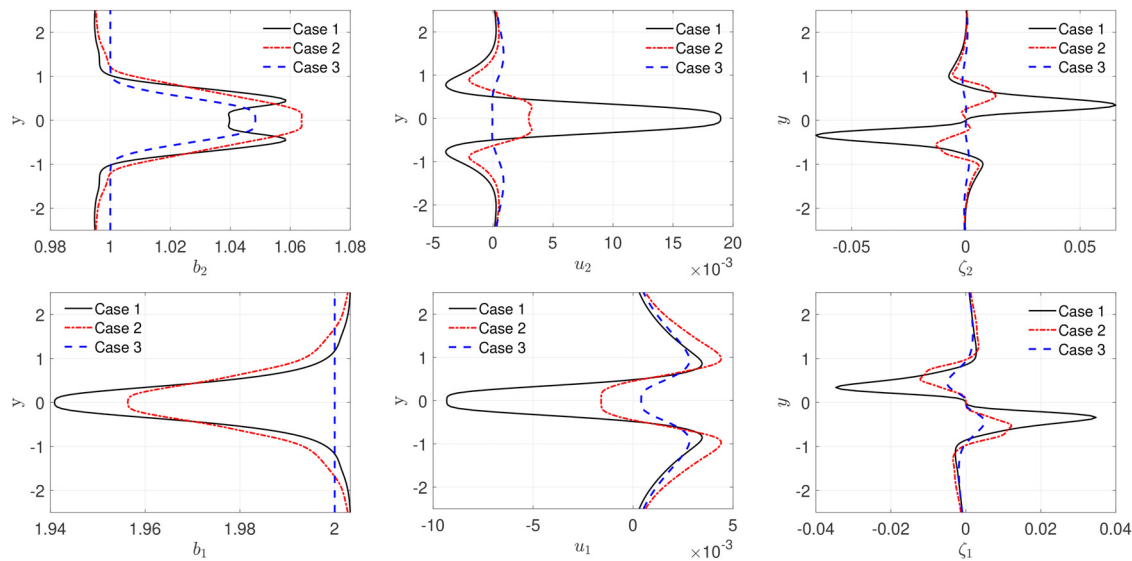


FIG. 4. Upper row: Zonally averaged b_2 , representing the buoyancy in the lower layer (left); u_2 , depicting the zonal velocity in the lower layer (middle), and ζ_2 , showing the relative vorticity in the lower layer (right). Lower row: Same as in the upper row, but for the upper layer.

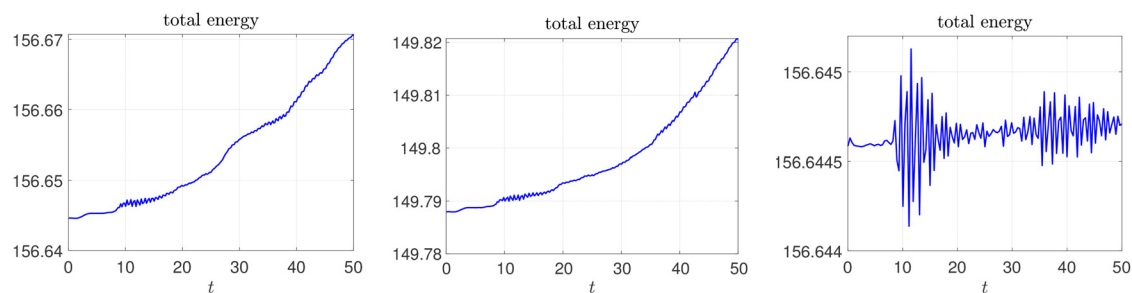


FIG. 5. Time evolution of the total energy in cases 1 (left), 2 (middle), and 3 (right).

respect to the Equator, although the center of the anomaly shifts slightly westward, and the buoyancy anomaly itself extends into the eastern portion of the system.

In addition to the vorticity and velocity diagnostics, in Fig. 5, we show the time evolution of the total energy in each case. As one sees, the moist-convective cases (cases 1 and 2) experience a more pronounced energy growth during the initial build-up phase compared to the dry case. This enhanced energy uptake is consistent with the vigorous convective processes that promote the formation of the *excited dipolar systems*. Furthermore, subsequent energy conversion from potential to kinetic energy is more efficient in the moist-convective environment, facilitating sustained eastward propagation.

A key finding from our numerical experiments—absent in previous mc(T)RSW model studies—is the emergence of a distinct *time lag mechanism* even under relatively weak moist-convective forcing. This lag, illustrated in Fig. 6, reflects the temporal gap between the system's initialization and the attainment of an excited threshold state capable

of sustained eastward propagation. Rather than exhibiting immediate response to imposed perturbations, the system undergoes a *build-up phase* characterized by slow and spatially nonuniform reorganization of energy, momentum, and moist static energy. This phase precedes the rapid amplification and eastward transition of organized structures and highlights a fundamentally nonlinear route to propagation onset. Specifically, the build-up is mediated by cumulative interactions between moist convective pulses and the ambient baroclinic environment. These interactions progressively enhance the vertical shear and facilitate the formation of coherent low-frequency structures, often in the form of moist-dipolar vortices, which are precursors to the eastward-propagating signal. From a dynamical standpoint, the delayed excitation suggests the presence of internal thresholds associated with convective heating accumulation and phase-locking of baroclinic modes. The system does not respond linearly to initial disturbances; instead, the convective source terms act intermittently and conditionally, only becoming effective once the background state

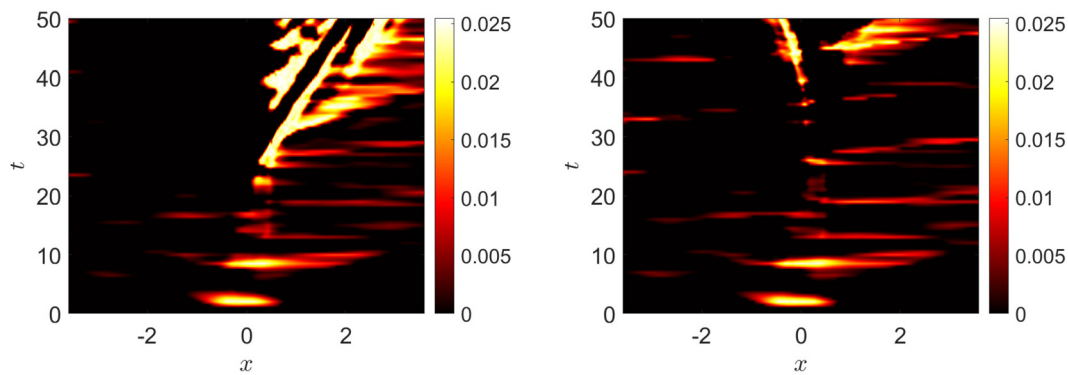


FIG. 6. Hovmöller diagrams of condensation C in cases 1 (left) and 2 (right) at $y = 0$.

approaches critical configurations in moisture, vertical shear, and potential vorticity gradients.

Moist convection thereby assumes a dual and evolving role throughout the life cycle: (i) as a net energy source, injecting latent heat and buoyancy into the lower layer, and (ii) as a structural organizer, incrementally aligning and amplifying perturbations in a manner that favors dipole formation and baroclinic coupling. These dipoles, once sufficiently developed, exhibit a self-sustaining eastward drift through momentum advection and wave-wave interaction, consistent with MJO-like features observed in tropical atmospheres.

The observed dynamics bear strong resemblance to the behavior of the MJO, particularly in terms of its initiation and propagation characteristics. The MJO exhibits a distinct time lag between the onset of convection and the development of coherent wave structures.^{52,53} Several studies have documented an anomalous sea surface temperature (SST) warming of 1–3 K in the equatorial Indian Ocean preceding

MJO initiation; see, e.g., Refs. 54–57. Notably, field observations from the dynamics of the MJO (DYNAMO) campaign⁵⁸ reveal that in the two weeks preceding an MJO event, the equatorial Indian Ocean experiences an SST anomaly of approximately 3 K.⁵⁹ This warming enhances boundary-layer moisture convergence, triggering a rapid release of latent heat flux and intensifying horizontal moisture advection; see also Refs. 60–62. Furthermore, studies have demonstrated that MJO activity is modulated by spatiotemporal variations in SST boundary forcing via air-sea interactions; see, e.g., Refs. 63–65.

Hovmöller diagrams of condensation in cases 1 and 2 (Fig. 6) depict two distinct systems: an excited system (left panel) and a semi-excited system (right panel). In case 1, the system exhibits higher phase velocities and enhanced eastward propagation, accompanied by stronger and more pronounced condensation fronts (see Fig. 7), which are characteristic of the *excited dipolar system*. The faster eastward propagation in case 1 reflects more vigorous convective activity, driven by

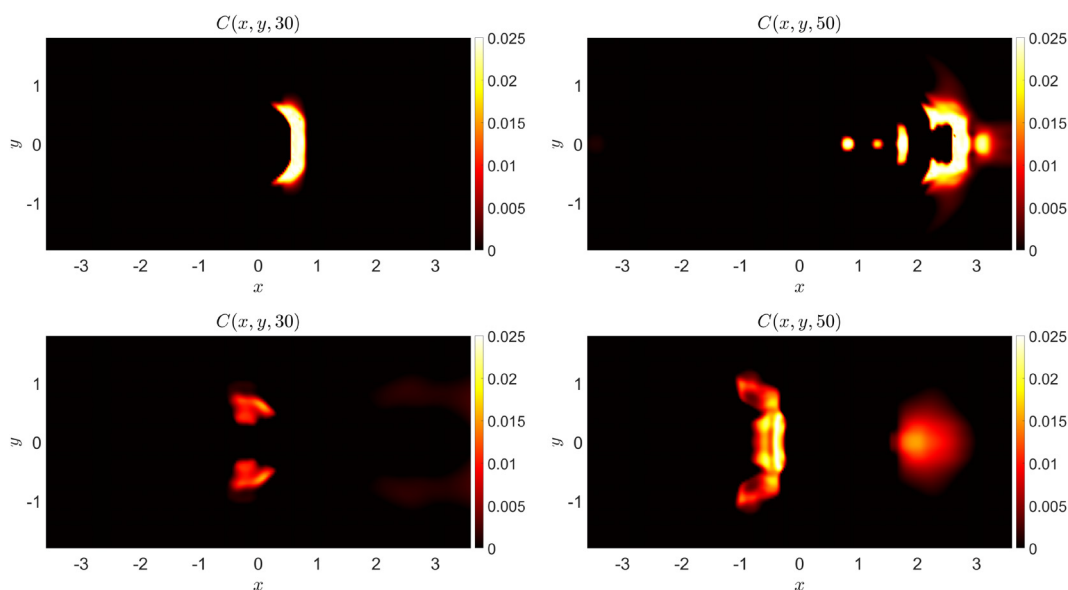


FIG. 7. Condensation patterns in cases 1 (upper row) and 2 (lower row) at $t = 30$ (left column) and $t = 50$ (right column).

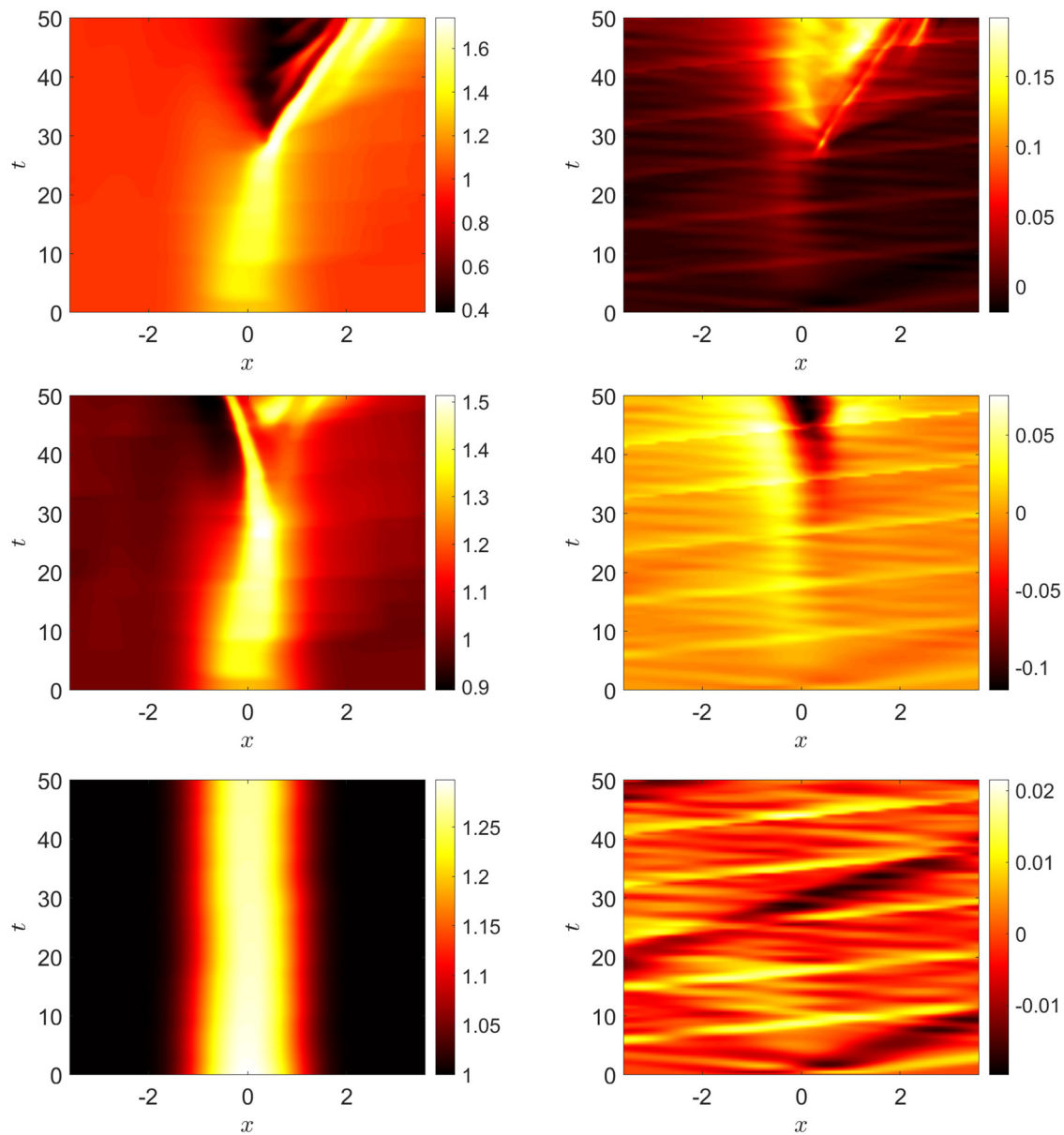


FIG. 8. Hovmöller diagrams of buoyancy b_2 (left column) and zonal velocity u_2 (right column) in cases 1 (upper row), 2 (middle row), and 3 (bottom row) at $y = 0$.

front cyclogenesis, leading to the rapid and intense development of organized wave structures. In contrast, the semi-excited system in case 2 exhibits a splitting of eastward and westward convective fluxes, as illustrated in Figs. 6 and 7. Similar to the vorticity pattern, which features multiple intensified dipolar structures, the condensation pattern of the *excited dipolar system* (Fig. 7) also displays multiple condensation fronts. Moreover, its front exhibits a temporally varying pattern, evolving in shape and amplitude over time, indicating variability in convective organization. Observational studies of MJO events have reported the existence of double rainband structures associated with

some MJO events,⁶⁶ further supporting these findings. Indeed, initial perturbations with zonally elongated aspect ratio structures enhance the excitation of an eastward-propagating system. This finding aligns with previous studies using different numerical models; see, e.g., Refs. 10 and 23–25.

The signature of eastward-propagating barotropic and baroclinic Kelvin waves is clearly evident in the lowest right panel of Fig. 8, which represents the equatorial adjustment of the *dry* case. The Hovmöller diagrams of zonal velocity and buoyancy for the fully excited system in case 1 (upper row in Fig. 8) show that the speed of eastward

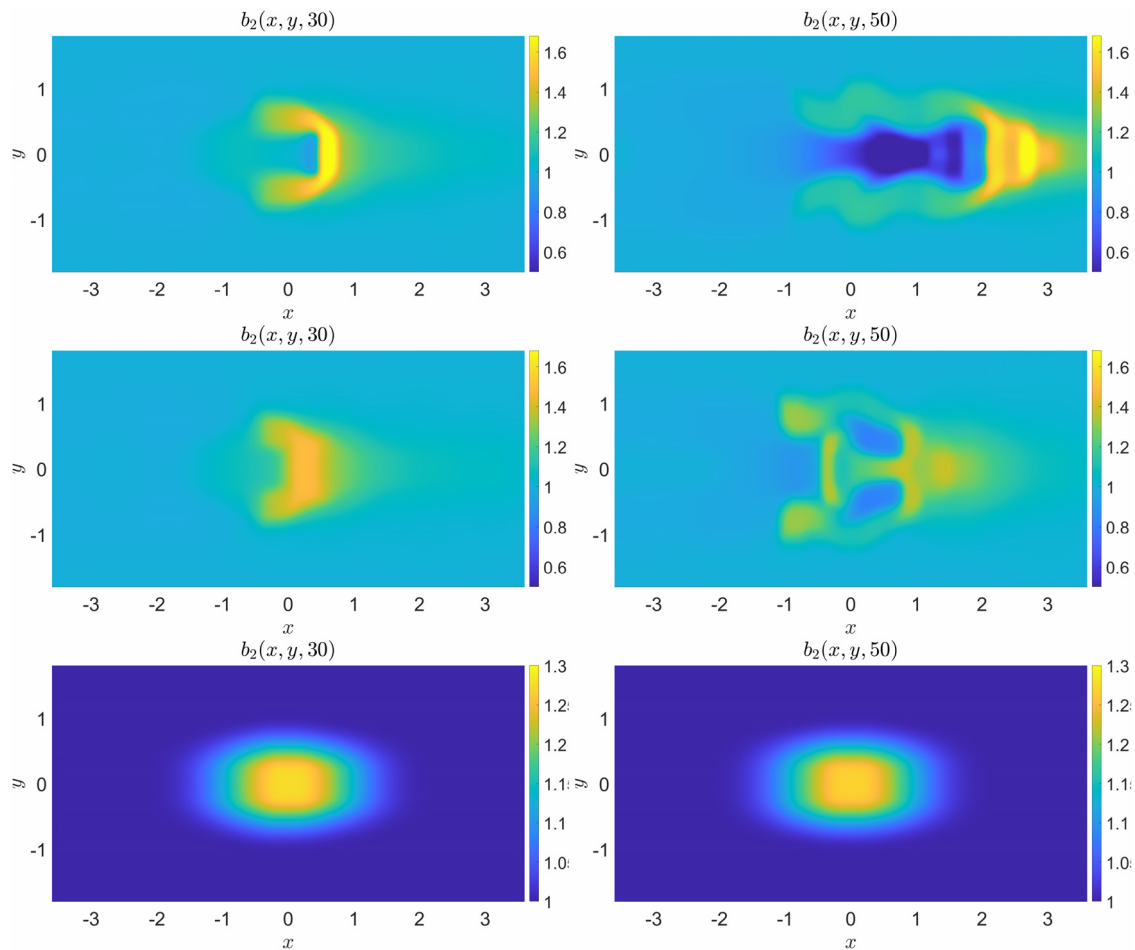


FIG. 9. Two snapshots of the buoyancy (b_2) field in the lower layer at $t = 30$ (left column) and $t = 50$ (right column) in cases 1 (top row), 2 (middle row), and 3 (bottom row).

propagation in this case is slower than that of the baroclinic Kelvin wave. This behavior is consistent with the dynamics observed in the Hovmöller diagram of condensation (Fig. 6, left), where the eastward propagation is also characterized by a lower speed compared to the pure baroclinic Kelvin wave.

A similar signature of eastward-propagating dynamics is seen in the Hovmöller diagrams of condensation in both cases 1 and 2 (Fig. 6), where the convectively coupled Kelvin wave influences condensation formation. This indicates that the moist-convective processes modulate the propagation but do not disrupt it abruptly. The presence of large-scale localized heating in moist-convective conditions contributes to the equatorial adjustment, but its impact on the eastward propagation of the barotropic Kelvin wave is minimal.

Interestingly, the formation of short-scale inertia-gravity waves behind the Kelvin front, as discussed in Fedorov and Melville,⁶⁷ does not dominate the eastward propagation process in the moist-convective systems studied here. These waves, typically formed in the wake of the Kelvin wave, are not a major factor in the eastward propagation dynamics, suggesting that the moist-convective environment primarily affects the wave's convective structure rather than influencing its speed or the characteristics of the barotropic component.

Further, Hovmöller diagrams of buoyancy b_2 (Fig. 8, left column) and snapshots of the buoyancy field (Fig. 9) in the lower layer reveal that *excited dipolar systems* are strongly associated with sharp, intense heatwave fronts governed by frontal geostrophic dynamics and exhibiting a pronounced east-west asymmetry. This distinctive east-west asymmetry in the temperature fronts has also been identified in satellite data from the cloud archive user system (CLAUS)⁶⁸ and in the dynamics of the MJO,⁶⁹ underscoring its critical role in tropical convective processes. Observational studies indicate that temperature anomalies linked to excited MJO events are significantly more intense than those found in typical MJO composite analyses.^{20,70} The splitting process observed in the condensation patterns of the semi-excited system (case 2) is also evident in the buoyancy field. The westward section of this splitting is coupled with Rossby waves. In contrast, the potential temperature anomaly field in the adiabatic case 3 remains almost stationary.

The ageostrophic component of the flow predominantly consists of inertia-gravity waves, which originate from the initial perturbation and regions of intense moist convection, subsequently radiating outward. As illustrated in Fig. 10, where we plot two snapshots of the divergence field in the lower layer, these waves exhibit strong

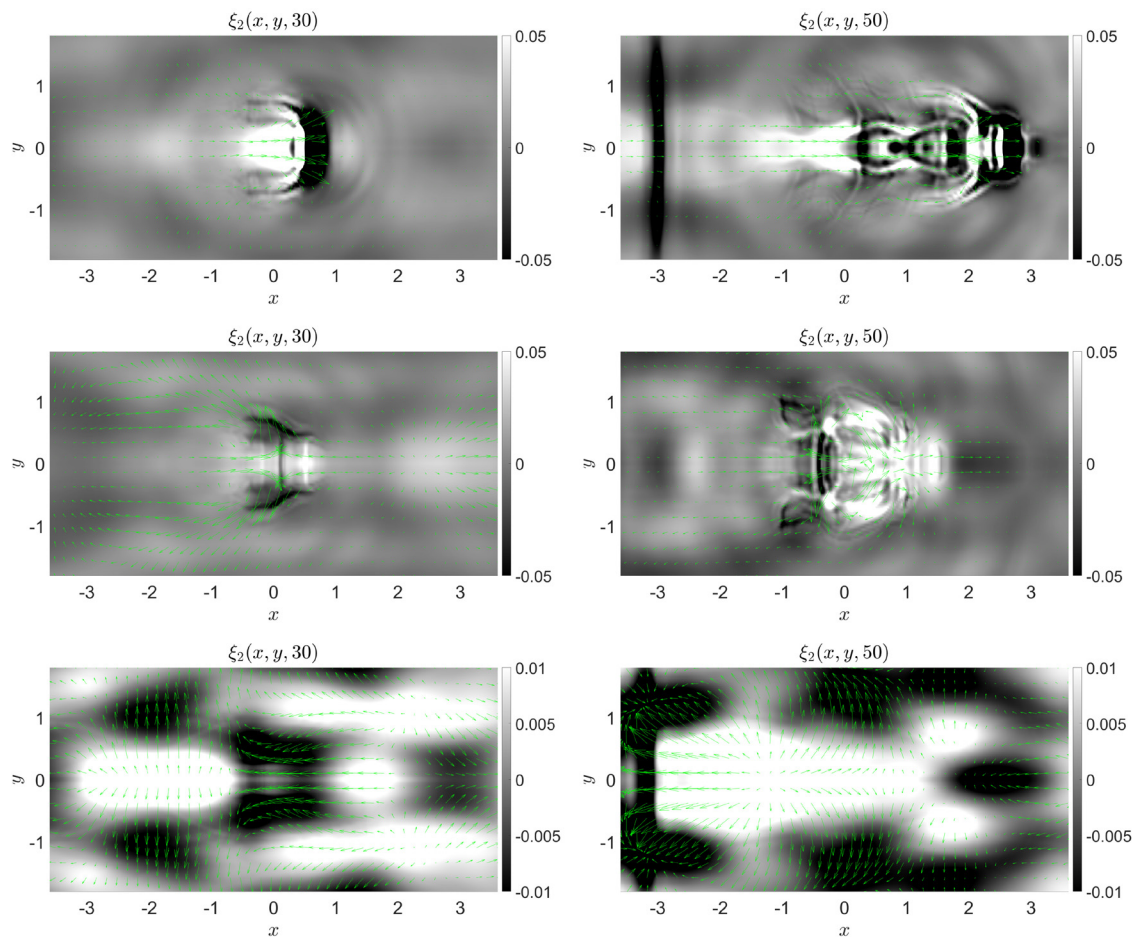


FIG. 10. Snapshots of the divergence field, $\xi_2 := (u_2)_x + (v_2)_y$, in the lower layer at $t = 30$ (left column) and $t = 50$ (right column) in cases 1 (top row), 2 (middle row), and 3 (bottom row).

convective coupling, with their amplitude significantly enhanced within the *excited dipolar system* of case 1. A key dynamical feature in this regime is the development of a well-defined convergence zone at the leading edge of the eastward-propagating waves, which facilitates

intensified condensation within the eastward-propagating dipolar structure near the equatorial center.

In contrast, case 2 is characterized by the formation of Rossby gyres, which induce westward-propagating convergence zones displaced off the Equator, as distinctly observed in Fig. 7. The equatorial-centered condensation process is accompanied by vertical advective transport, which has been linked to the formation of cumulus congestus clouds and contributes to mid-tropospheric moistening.^{71,72} Additional sensitivity experiments, involving variations in grid resolution and minor perturbations of the initial amplitude, confirmed that the emergence of the excited dipolar systems is robust. While small quantitative differences were observed, the overall qualitative behavior and the transition from Gill-like to monsoon-like responses remain consistent.

IV. CONCLUSION AND DISCUSSION

By presenting a sequence of causal relationships, this study reconciles two previously divergent theories of MJO dynamics: (1) the traditional view emphasizing moisture accumulation, extreme precipitation, and moist convection as necessary precursors for MJO

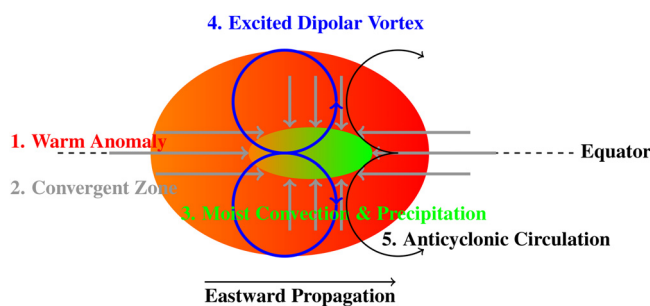


FIG. 11. Schematic illustration of the *excited dipolar system* and the resulting MJO-like structure formation over the Equator.

initiation,^{19,21,22,28,73} and (2) the more recent modon-based framework.^{11,17} We demonstrate that these modons manifest as self-propelled *excited dipolar systems* within the moist-convective environment. Our analysis identifies a well-defined temporal hierarchy: positive buoyancy anomalies trigger the initial phase, followed sequentially by (i) moisture accumulation and (ii) the emergence of *excited dipolar systems*, ultimately leading to MJO genesis and propagation (Fig. 11). While several studies have emphasized the accumulation of moisture to the east of the MJO convective center as a key prerequisite for its eastward propagation (see, e.g., Refs. 74–81), the genesis mechanism proposed in the current framework reinterprets the causal chains (Fig. 11) such that this moist convection emerges as a secondary consequence rather than a primary driver. Specifically, within this causal hierarchy (Fig. 11), the initiation of an MJO-like structure is fundamentally governed by the nonlinear relaxation dynamics of large-scale buoyancy anomalies, which then create conditions favorable for eastward moisture advection and preconditioning. Thus, instead of serving as an external prerequisite, the moisture buildup behind the convective envelope is an intrinsic component of the self-sustaining cycle, reinforcing propagation through feedback mechanisms that amplify the convective response. These findings are consistent with the MJO-like genesis theory proposed in Rostami and Zeitlin²³ and Rostami *et al.*,²⁴ which, after minor refinements, can be summarized as follows.

A. Refined theory of the genesis of MJO-like structures

An eastward-propagating MJO-like structure can emerge in a self-sustained and self-propelled manner through the nonlinear relaxation (adjustment) of a large-scale positive buoyancy anomaly, a depressed anomaly, or a combination of both. This process is initiated once the anomaly reaches a critical threshold in the presence of moist convection near the Equator. The resulting MJO-like episode manifests as a convectively coupled excited dipolar system, characterized by an enhanced vortex pair that induces counter-rotating anticyclones, accompanied by weaker opposite-sign counterparts in the upper layer. This structure interacts with a convectively coupled baroclinic Kelvin wave, which propagates at a higher phase speed than the dipolar system and operates on an intraseasonal timescale.

ACKNOWLEDGMENTS

The work of Y. Cao was supported in part by the Guangdong Basic and Applied Basic Research Foundation (Grant No. 2025A1515012249), A. Kurganov by NSFC Grant Nos. 12171226 and W2431004, and Y. Liu by SNFS Grant Nos. 200020-204917 and FZEB-0-166980. M. Rostami gratefully acknowledges funding from Virgin Unite USA, Inc., through the Planetary Boundary Science Lab.

AUTHOR DECLARATIONS

Conflict of Interest

The authors have no conflicts to disclose.

Author Contributions

Yangyang Cao: Conceptualization (equal); Data curation (equal); Formal analysis (equal); Funding acquisition (equal); Investigation (equal); Methodology (equal); Project administration (equal);

Resources (equal); Software (equal); Validation (equal); Visualization (equal); Writing – review & editing (equal). **Alexander Kurganov:** Conceptualization (equal); Data curation (equal); Formal analysis (equal); Funding acquisition (equal); Investigation (equal); Methodology (equal); Project administration (equal); Resources (equal); Software (equal); Supervision (equal); Validation (equal); Visualization (equal); Writing – review & editing (equal). **Yongle Liu:** Conceptualization (equal); Data curation (equal); Formal analysis (equal); Funding acquisition (equal); Investigation (equal); Methodology (equal); Software (equal); Validation (equal); Visualization (equal); Writing – review & editing (equal). **Masoud Rostami:** Conceptualization (equal); Data curation (equal); Formal analysis (equal); Funding acquisition (equal); Investigation (equal); Methodology (equal); Software (equal); Supervision (equal); Validation (equal); Visualization (equal); Writing – original draft (equal). **Vladimir Zeitlin:** Conceptualization (equal); Investigation (equal); Methodology (equal); Supervision (equal); Validation (equal); Visualization (equal).

DATA AVAILABILITY

The data that support the findings of this study are available from the corresponding author upon reasonable request.

REFERENCES

- 1A. E. Gill, *Atmosphere-Ocean Dynamics, Volume 30 of International Geophysics Series* (Academic Press, 1982).
- 2V. Zeitlin, *Geophysical Fluid Dynamics: Understanding (Almost) Everything with Rotating Shallow Water Models* (Oxford University Press, Oxford, 2018).
- 3A. E. Gill, "Some simple solutions for heat-induced tropical circulation," *Q. J. R. Meteorol. Soc.* **106**(449), 447–462 (1980).
- 4F. Bouchut, J. Lambaerts, G. Lapeyre, and V. Zeitlin, "Fronts and nonlinear waves in a simplified shallow-water model of the atmosphere with moisture and convection," *Phys. Fluids* **21**(11), 116604 (2009).
- 5J. Lambaerts, G. Lapeyre, and V. Zeitlin, "Moist versus dry barotropic instability in a shallow-water model of the atmosphere with moist convection," *J. Atmos. Sci.* **68**, 1234–1252 (2011).
- 6J. Lambaerts, G. Lapeyre, V. Zeitlin, and F. Bouchut, "Simplified two-layer models of precipitating atmosphere and their properties," *Phys. Fluids* **23**(4), 046603 (2011).
- 7J. Lambaerts, G. Lapeyre, and V. Zeitlin, "Moist versus dry baroclinic instability in a simplified two-layer atmospheric model with condensation and latent heat release," *J. Atmos. Sci.* **69**, 1405–1426 (2012).
- 8M. Rostami and V. Zeitlin, "Influence of condensation and latent heat release upon barotropic and baroclinic instabilities of vortices in a rotating shallow water f -plane model," *Geophys. Astrophys. Fluid Dyn.* **111**(1), 1–31 (2017).
- 9M. Rostami and V. Zeitlin, "An improved moist-convective rotating shallow-water model and its application to instabilities of hurricane-like vortices," *Q. J. R. Meteorol. Soc.* **144**(714), 1450–1462 (2018).
- 10M. Rostami and V. Zeitlin, "Geostrophic adjustment on the equatorial beta-plane revisited," *Phys. Fluids* **31**(8), 081702 (2019).
- 11M. Rostami and V. Zeitlin, "Eastward-moving convection-enhanced modons in shallow water in the equatorial tangent plane," *Phys. Fluids* **31**, 021701 (2019).
- 12M. Rostami and V. Zeitlin, "Eastward-moving equatorial modons in moist-convective shallow-water models," *Geophys. Astrophys. Fluid Dyn.* **115**(3), 345–367 (2021).
- 13B. Zhao, V. Zeitlin, and A. V. Fedorov, "Equatorial modons in dry and moist-convective shallow-water systems on a rotating sphere," *J. Fluid Mech.* **916**, A8 (2021).
- 14N. Lahaye, O. Larroque, and V. Zeitlin, "Equatorial modons in thermal rotating shallow water model," *J. Fluid Mech.* **984**, A58 (2024).
- 15J. P. Boyd, "Equatorial solitary waves. Part 3: Westward-traveling modons," *J. Phys. Oceanogr.* **15**(1), 46–54 (1985).

- ¹⁶V. D. Larichev and G. M. Reznik, "Two-dimensional solitary Rossby waves," *Dokl. Akad. Nauk. SSSR* **231**, 1077–1079 (1976).
- ¹⁷J.-I. Yano and J. J. Tribbia, "Tropical atmospheric Madden-Julian Oscillation: A strongly nonlinear free solitary Rossby wave?" *J. Atmos. Sci.* **74**(10), 3473–3489 (2017).
- ¹⁸T. Matsuno, "Quasi-geostrophic motions in the equatorial area," *J. Meteorol. Soc. Jpn.* **44**(1), 25–43 (1966).
- ¹⁹R. A. Madden and P. R. Julian, "Description of global-scale circulation cells in the tropics with a 40–50 day period," *J. Atmos. Sci.* **29**(6), 1109–1123 (1972).
- ²⁰G. N. Kiladis, K. H. Straub, and P. T. Haertel, "Zonal and vertical structure of the Madden-Julian Oscillation," *J. Atmos. Sci.* **62**(8), 2790–2809 (2005).
- ²¹R. A. Madden, "Seasonal variations of the 40–50 day oscillation in the tropics," *J. Atmos. Sci.* **43**(24), 3138–3158 (1986).
- ²²R. A. Madden and P. R. Julian, "Observations of the 40–50-day tropical oscillation—A review," *Mon. Weather Rev.* **122**(5), 814–837 (1994).
- ²³M. Rostami and V. Zeitlin, "Can geostrophic adjustment of baroclinic disturbances in the tropical atmosphere explain MJO events?" *Q. J. R. Meteorol. Soc.* **146**(733), 3998–4013 (2020).
- ²⁴M. Rostami, B. Zhao, and S. Petri, "On the genesis and dynamics of Madden-Julian oscillation-like structure formed by equatorial adjustment of localized heating," *Q. J. R. Meteorol. Soc.* **148**(749), 3788–3813 (2022).
- ²⁵Y. Liang, A. V. Fedorov, V. Zeitlin, and P. Haertel, "Excitation of the Madden-Julian Oscillation in atmospheric adjustment to equatorial heating," *J. Atmos. Sci.* **78**(12), 3933–3950 (2021).
- ²⁶M. F. Khairoutdinov and D. A. Randall, "A cloud resolving model as a cloud parameterization in the NCAR Community Climate System Model: Preliminary results," *Geophys. Res. Lett.* **28**(18), 3617–3620, <https://doi.org/10.1029/2001GL013552> (2001).
- ²⁷L. Yu and A. V. Fedorov, "Excitation of the Madden-Julian Oscillation in response to transient ocean warming in SPCAM," *Geophys. Res. Lett.* **49**(22), e2022GL100853, <https://doi.org/10.1029/2022GL100853> (2022).
- ²⁸X. Jiang, A. F. Adames, D. Kim, E. D. Maloney, H. Lin, H. Kim, C. Zhang, C. A. DeMott, and N. P. Klingaman, "Fifty years of research on the Madden-Julian Oscillation: Recent progress, challenges, and perspectives," *JGR. Atmos.* **125**(17), e2019JD030911 (2020).
- ²⁹C. Zhang, A. F. Adames, B. Khouider, B. Wang, and D. Yang, "Four theories of the Madden-Julian Oscillation," *Rev. Geophys.* **58**(3), e2019RG000685, <https://doi.org/10.1029/2019RG000685> (2020).
- ³⁰M. Rostami, S. Petri, B. Fallah, and F. Fazel-Rastgar, "Aeolus 2.0's thermal rotating shallow water model: A new paradigm for simulating extreme heatwaves, westerly jet intensification, and more," *Phys. Fluids* **37**(1), 016604 (2025).
- ³¹A. Kurganov, Y. Liu, and V. Zeitlin, "Moist-convective thermal rotating shallow water model," *Phys. Fluids* **32**(6), 066601 (2020).
- ³²M. Rostami, S. Petri, B. Fallah, and F. Fazel-Rastgar, "A novel sea surface evaporation scheme assessed by the thermal rotating shallow water model," *Atmos. Sci. Lett.* **26**(1), e1287 (2025).
- ³³P. Ripa, "Conservation laws for primitive equations models with inhomogeneous layers," *Geophys. Astrophys. Fluid Dyn.* **70**(1–4), 85–111 (1993).
- ³⁴G. DalMaso, P. L. Floch, and F. Murat, "Definition and weak stability of non-conservative products," *J. Math. Pure. Appl.* **74**, 483–548 (1995).
- ³⁵P. G. LeFloch, *Hyperbolic Systems of Conservation Laws. The Theory of Classical and Nonclassical Shock Waves* (Birkhäuser Verlag, Basel, 2002).
- ³⁶C. Parés, "Numerical methods for nonconservative hyperbolic systems: A theoretical framework," *SIAM J. Numer. Anal.* **44**(1), 300–321 (2006).
- ³⁷M. J. Castro, P. G. LeFloch, M. L. Muñoz-Ruiz, and C. Parés, "Why many theories of shock waves are necessary: Convergence error in formally path-consistent schemes," *J. Comput. Phys.* **227**(17), 8107–8129 (2008).
- ³⁸M. J. Castro, T. Morales de Luna, and C. Parés, "Well-balanced schemes and path-conservative numerical methods," in *Handbook of Numerical Methods for Hyperbolic Problems* (Elsevier/North-Holland, Amsterdam, 2017), Vol. 18, pp. 131–175.
- ³⁹C. Parés, "Path-conservative numerical methods for nonconservative hyperbolic systems," in *Numerical Methods for Balance Laws* (Dept. Math., Seconda University Napoli, Caserta, 2009), Vol. 24, pp. 67–121.
- ⁴⁰Y. Cao, A. Kurganov, Y. Liu, and V. Zeitlin, "Flux globalization based well-balanced path-conservative central upwind scheme for two-layer thermal rotating shallow water equations," *J. Comput. Phys.* **474**, 111790 (2023).
- ⁴¹Y. Cao, A. Kurganov, Y. Liu, and V. Zeitlin, "Flux globalization-based well-balanced path-conservative central-upwind scheme for two-dimensional two-layer thermal rotating shallow water equations," *J. Comput. Phys.* **515**, 113273 (2024).
- ⁴²A. Chertock, S. Cui, A. Kurganov, and T. Wu, "Steady state and sign preserving semi-implicit Runge-Kutta methods for ODEs with stiff damping term," *SIAM J. Numer. Anal.* **53**(4), 2008–2029 (2015).
- ⁴³J. P. Boyd, "The nonlinear equatorial Kelvin wave," *J. Phys. Oceanogr.* **10**(1), 1–11 (1980).
- ⁴⁴J. L. Sommer, G. M. Reznik, and V. Zeitlin, "Nonlinear geostrophic adjustment of long-wave disturbances in the shallow water model on the equatorial beta-plane," *J. Fluid Mech.* **515**, 135–170 (2004).
- ⁴⁵P. Ripa, "Nonlinear wave-wave interactions in a one-layer reduced-gravity model on the equatorial β plane," *J. Phys. Oceanogr.* **12**(1), 97–111 (1982).
- ⁴⁶G. M. Reznik, V. Zeitlin, and M. Ben Jelloul, "Nonlinear theory of geostrophic adjustment. I. Rotating shallow-water model," *J. Fluid Mech.* **445**, 93–120 (2001).
- ⁴⁷M. Rostami, L. Severino, S. Petri, and S. Hariri, "Dynamics of localized extreme heatwaves in the mid-latitude atmosphere: A conceptual examination," *Atmos. Sci. Lett.* **25**(1), e1188 (2024).
- ⁴⁸V. Zeitlin, G. M. Reznik, and M. Ben Jelloul, "Nonlinear theory of geostrophic adjustment. II. Two-layer and continuously stratified primitive equations," *J. Fluid Mech.* **491**, 207–228 (2003).
- ⁴⁹M. Rostami and V. Zeitlin, "Evolution, propagation and interactions with topography of hurricane-like vortices in a moist-convective rotating shallow-water model," *J. Fluid Mech.* **902**, A24 (2020).
- ⁵⁰B. Wang, G. Chen, and F. Liu, "Diversity of the Madden-Julian Oscillation," *Sci. Adv.* **5**(7), eaax0220 (2019).
- ⁵¹D. Wang, J.-I. Yano, and Y. Lin, "Madden-Julian oscillations seen in the upper-troposphere vorticity field: Interactions with Rossby wave trains," *J. Atmos. Sci.* **76**(6), 1785–1807 (2019).
- ⁵²C. A. Hoopes, L. L. Hood, and T. J. Galarneau, Jr., "Lagged response of MJO convection and precipitation to solar ultraviolet variations on intraseasonal time scales," *Geophys. Res. Lett.* **51**(11), e2023GL107701, <https://doi.org/10.1029/2023GL107701> (2024).
- ⁵³S. R. Kemball-Cook and B. C. Weare, "The onset of convection in the Madden-Julian Oscillation," *J. Clim.* **14**(5), 780–793 (2001).
- ⁵⁴C. A. DeMott, N. P. Klingaman, and S. J. Woolnough, "Atmosphere-ocean coupled processes in the Madden-Julian oscillation," *Rev. Geophys.* **53**(4), 1099–1154, <https://doi.org/10.1002/2014RG000478> (2015).
- ⁵⁵M. Flatau, P. J. Flatau, P. Phoebus, and P. P. Niiler, "The feedback between equatorial convection and local radiative and evaporative processes: The implications for intraseasonal oscillations," *J. Atmos. Sci.* **54**(19), 2373–2386 (1997).
- ⁵⁶A. J. Matthews, "Primary and successive events in the Madden-Julian oscillation," *Q. J. R. Meteorol. Soc.* **134**(631), 439–453 (2008).
- ⁵⁷T. Shinoda, H. H. Hendon, and J. Glick, "Intraseasonal variability of surface fluxes and sea surface temperature in the tropical western Pacific and Indian Oceans," *J. Clim.* **11**(7), 1685–1702 (1998).
- ⁵⁸K. Yoneyama, C. Zhang, and C. N. Long, "Tracking pulses of the Madden-Julian Oscillation," *Bull. Amer. Meteorol. Soc.* **94**(12), 1871–1891 (2013).
- ⁵⁹J. N. Moum, S. P. de Szoeke, W. D. Smyth, J. B. Edson, H. L. DeWitt, A. J. Moulin, E. J. Thompson, C. J. Zappa, S. A. Rutledge, R. H. Johnson, and C. W. Fairall, "Air-sea interactions from westerly wind bursts during the November 2011 MJO in the Indian Ocean," *Bull. Amer. Meteorol. Soc.* **95**(8), 1185–1199 (2014).
- ⁶⁰T. Li, C. Zhao, P.-C. Hsu, and T. Nasuno, "MJO initiation processes over the tropical Indian Ocean during DYNAMO/CINDY2011," *J. Clim.* **28**(6), 2121–2135 (2015).
- ⁶¹A. V. Rydbeck and T. G. Jensen, "Oceanic impetus for convective onset of the Madden-Julian Oscillation in the Western Indian Ocean," *J. Clim.* **30**(11), 4299–4316 (2017).
- ⁶²C. Zhao, T. Li, and T. Zhou, "Precursor signals and processes associated with MJO initiation over the tropical Indian Ocean," *J. Clim.* **26**(1), 291–307 (2013).
- ⁶³H.-M. Kim, C. D. Hoyos, P. J. Webster, and I.-S. Kang, "Sensitivity of MJO simulation and predictability to sea surface temperature variability," *J. Clim.* **21**(20), 5304–5317 (2008).

- ⁶⁴K. Pegion and B. P. Kirtman, "The impact of air–sea interactions on the simulation of tropical intraseasonal variability," *J. Clim.* **21**(24), 6616–6635 (2008).
- ⁶⁵C. Stan, "The role of SST variability in the simulation of the MJO," *Clim. Dyn.* **51**(7), 2943–2964 (2018).
- ⁶⁶L. Zhu and T. Li, "A special MJO event with a double Kelvin wave structure," *J. Meteorol. Res.* **31**(2), 295–308 (2017).
- ⁶⁷A. V. Fedorov and W. K. Melville, "Kelvin fronts on the equatorial thermocline," *J. Phys. Oceanogr.* **30**(7), 1692–1705 (2000).
- ⁶⁸K. I. Hodges, D. W. Chappell, G. J. Robinson, and G. Yang, "An improved algorithm for generating global window brightness temperatures from multiple satellite infrared imagery," *J. Atmos. Ocean. Technol.* **17**(10), 1296–1312 (2000).
- ⁶⁹V. C. Mayta and A. F. Adames, "Moist thermodynamics of convectively coupled waves over the Western Hemisphere," *J. Clim.* **36**(9), 2765–2780 (2023).
- ⁷⁰C. Zhang, "Madden-Julian oscillation," *Rev. Geophys.* **43**(2), RG2003, <https://doi.org/10.1029/2004RG000158> (2005).
- ⁷¹G. N. Kiladis, M. C. Wheeler, P. T. Haertel, K. H. Straub, and P. E. Roundy, "Convectively coupled equatorial waves," *Rev. Geophys.* **47**(2), RG2003, <https://doi.org/10.1029/2008RG000266> (2009).
- ⁷²B. Wang and H. Rui, "Dynamics of the coupled moist Kelvin–Rossby wave on an equatorial β -plane," *J. Atmos. Sci.* **47**(4), 397–413 (1990).
- ⁷³C. Jones, D. E. Waliser, K. M. Lau, and W. Stern, "Global occurrences of extreme precipitation and the Madden–Julian Oscillation: Observations and predictability," *J. Clim.* **17**(23), 4575–4589 (2004).
- ⁷⁴A. F. Adames and J. M. Wallace, "Three-dimensional structure and evolution of the moisture field in the MJO," *J. Atmos. Sci.* **72**(10), 3733–3754 (2015).
- ⁷⁵J. A. Andersen and Z. Kuang, "Moist static energy budget of MJO-like disturbances in the atmosphere of a zonally symmetric aquaplanet," *J. Clim.* **25**(8), 2782–2804 (2012).
- ⁷⁶H. Kim, M. A. Janiga, and K. Pegion, "MJO propagation processes and mean biases in the SubX and S2S reforecasts," *JGR. Atmos.* **124**(16), 9314–9331 (2019).
- ⁷⁷A. J. Majda and S. N. Stechmann, "The skeleton of tropical intraseasonal oscillations," *Proc. Natl. Acad. Sci. U. S. A.* **106**(21), 8417–8422 (2009).
- ⁷⁸A. J. Majda and S. N. Stechmann, "Nonlinear dynamics and regional variations in the MJO skeleton," *J. Atmos. Sci.* **68**(12), 3053–3071 (2011).
- ⁷⁹E. D. Maloney, "The moist static energy budget of a composite tropical intraseasonal oscillation in a climate model," *J. Clim.* **22**(3), 711–729 (2009).
- ⁸⁰A. Sobel and E. Maloney, "Moisture nodes and the eastward propagation of the MJO," *J. Atmos. Sci.* **70**(1), 187–192 (2013).
- ⁸¹A. Sobel, S. Wang, and D. Kim, "Moist static energy budget of the MJO during DYNAMO," *J. Atmos. Sci.* **71**(11), 4276–4291 (2014).